Shear flow near solids: Epitaxial order and flow boundary conditions

Peter A. Thompson
Department of Physics and Astronomy, The Johns Hopkins University, Baltimore, Maryland 21218

Mark O. Robbins
Department of Physics and Astronomy, The Johns Hopkins University, Baltimore, Maryland 21218 and Institute for Theoretical Physics, University of California, Santa Barbara, California 93106

(Received 22 January 1990)

We report on molecular-dynamics simulations of Lennard-Jones liquids sheared between two solid walls. The velocity fields, flow boundary conditions, and fluid structure were studied for a variety of wall and fluid properties. A broad spectrum of boundary conditions was observed including slip, no-slip, and locking. We show that the degree of slip is directly related to the amount of structure induced in the fluid by the periodic potential from the solid walls. For weak wall-fluid interactions there is little ordering and slip was observed. At large interactions, substantial epitaxial ordering was induced and the first one or two fluid layers became locked to the wall. This epitaxial ordering was enhanced when the wall and fluid densities were equal. For unequal densities, high-order commensurate structures formed in the first fluid layer creating slip *within* the fluid.

I. INTRODUCTION

One of the fundamental assumptions in fluid mechanical formulations of Newtonian flow past solids is the "no-slip" boundary condition (BC): that is, that the tangential component of the fluid velocity equals that of the solid at the surface. However, the microscopic origin of the no-slip condition has remained elusive for over a century. While experiments at macroscopic scales are consistent with this BC, recent experiments which probe molecular scales indicate that the BC may be different.[1-3] An understanding of flow at these scales is essential to theories of lubrication, flow in porous media, and the spreading of fluids.

The primary difficulty impeding a theoretical understanding of flow near solid surfaces lies with the limitations of kinetic theory.[4] A rigorous treatment should make no assumptions about the BC. This would require including multiple scattering of fluid atoms from individual wall molecules, which is not feasible analytically. An alternative approach, which has become realizable with the advent of modern supercomputers, is nonequilibrium molecular-dynamics (MD) simulations. In studying microscopic transport properties, the MD approach has significant advantages over kinetic theory. For example, multiple scattering is included explicitly, and no assumptions have to be made regarding the molecular distribution function.

Recently, nonequilibrium MD simulations of simple fluids have been used to study Newtonian flow near solid boundaries.[4-9] They have included investigations of ideal Pouiselle[4-6] and Couette flow,[4,7-9] as well as flow through small pores.[7,8] Early studies used various types of "structureless" walls and observed only slip BC's.[8] More realistic simulations, with walls composed of atoms arranged on a lattice, revealed more complex BC's. In most cases,[4-5,9] locking between wall and fluid was observed: The velocity in the liquid reached that of the wall one or two molecular spacings *inside the liquid.* Recent studies showed that this distance increased with the strength of wall-fluid interactions,[5,9] and decreased with temperature.[5] Experiments also indicate a variety of BC's may occur, ranging from locking[1] to slip.[2]

In this paper, we present a detailed analysis of the velocity fields and fluid structure near solid boundaries. In particular, we focus on how wall-induced structure in the fluid affects flow. Earlier studies[7] attempted to correlate modulations in the fluid density perpendicular to the wall with the velocity BC's. We find that two-dimensional ordering *parallel* to the wall is far more significant. The wall produces a periodic potential in the fluid with a characteristic strength and period. Increasing the strength induces epitaxial ordering in the fluid layers near the wall, and the BC reflects this locking. These locked layers correspond to a solid phase wetting the substrate. Wall and fluid become decoupled when the potential is weak, and slip occurs. The crossover from locking to slip depends on the commensurability of wall and fluid densities. Unusual boundary conditions can arise at intermediate strengths and unequal densities. For example, we observed slip *within* the fluid when the wall induced high-order commensurate structure in the first fluid layer.

In the next section we describe the simulation techniques used in our study. We then discuss layering of fluids normal to the wall. This layering produces oscillations in the velocity, stress, and other variables. However, we show that averaging these microscopic quantities within fluid layers produces smoothly varying functions which can be described by macroscopic hydrodynamics. We next describe the observed flow BC's, and correlate them to the structure induced in the fluid parallel to the wall. Section IV presents a summary and conclusions.

II. SIMULATION GEOMETRY AND METHOD

Our simulations were performed in a Couette geometry (Fig. 1). The fluid was confined between two solid planar

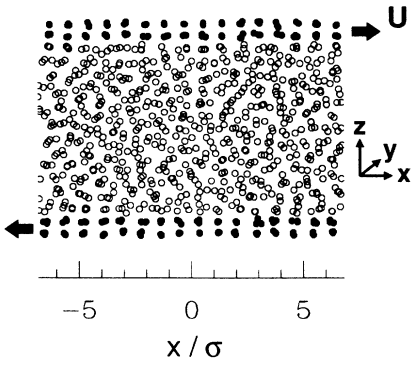

FIG. 1. Projections of particle positions onto the xz plane for $U=1\sigma\tau^{-1}$, $\varepsilon_{wf}=\varepsilon$, $\rho_w=\rho$, and $\langle\delta u^2\rangle=0.01d^2$. There are $N_f=672$ fluid atoms and $N_w=192$ wall atoms. The distance between solid walls is 12.8σ.

walls parallel to the xy plane with periodic BC's imposed along the x and y axes. Couette flow was generated by moving the walls at constant velocity U in opposite directions along the x axis. Each wall consisted of atoms forming two [001] planes of an fcc lattice. To maintain a well-defined solid structure with a minimum number of solid atoms, each wall atom was attached to a lattice site with a spring. The spring constant κ controlled the thermal roughness of the wall and its responsiveness to the fluid. κ was adjusted so that the mean-squared displacement about the lattice sites $\langle\delta u^2\rangle$ was less than the Lindemann criterion[10] for melting: $\langle\delta u^2\rangle/d^2<0.023$, where d is the nearest-neighbor distance. For the results shown, we used $\langle\delta u^2\rangle/d^2=0.01$ or 0.

The interactions between fluid atoms were modeled using a Lennard-Jones (LJ) potential,

$$V_{\rm LJ}(r)=4\varepsilon[(\sigma/r)^{12}-(\sigma/r)^6]\ , \tag{1}$$

where r is the distance separating the atoms, and ε and σ define the characteristic energy and length scales of the fluid. This potential is easy to compute and has been well studied. In addition, recent nonequilibrium MD simulations of LJ fluids have shown that relatively small systems ($\sim$1000 atoms) reproduce many aspects of macroscopic fluid dynamics.[4–9,11] A LJ potential with energy and length scales ε_{wf} and σ_{wf} was also used for interactions between wall and fluid atoms.

To reduce computation time, $V_{\rm LJ}$ was truncated at $r_c=2.2\sigma$. Results obtained for $r_c=3\sigma$ were the same within statistical fluctuations. Thus beyond these cutoffs the potential is negligible compared to thermal energies. However, decreasing r_c to 2σ or 1.8σ produced significant changes in the potential, BC's, and even the fluid viscosity.

The fluid temperature and density in most simulations were fixed at $k_BT/\varepsilon=1.1$ and $\rho\sigma^3=0.81$. This represents a compressed fluid about 30% above the melting temperature. We then examined the variation of fluid structure and velocity fields with changes in the effective corrugation of the wall. The strength of the corrugation was varied by changing $\varepsilon_{wf}/\varepsilon$ at fixed $\sigma_{wf}/\sigma=1$. Two wall densities, $\rho_w/\rho=1$ and 2.52, were studied to examine the effect of wall-fluid commensurability.

Standard MD techniques were used.[12] The equations of motion were integrated using a fifth-order Gear predictor-corrector algorithm with a time step of 0.005τ, where $\tau=(m\sigma^2/\varepsilon)^{1/2}$. The layered link-cell method of Grest, Dunweg, and Kremer[13] was used to reduce the computational effort involved in calculating interatomic forces. A typical run at $U=1\sigma\tau^{-1}$ required approximately 100τ to stabilize and 200τ for averaging. At lower U or higher temperatures, additional averaging was necessary to reduce thermal fluctuations.

Shearing the fluid introduces viscous dissipation which gradually heats the system. A common method for removing heat in MD simulations[12] entails the *ad hoc* rescaling of the instantaneous atomic velocities $\mathbf{v}$. However, when the steady-state flow field is not known *a priori*, velocity rescaling may bias the flow field.[14] Heinbuch and Fischer recently observed this short of biasing in simulations of flow through small pores.[5] To avoid this problem, we maintained constant temperature by adding damping and Langevin noise terms[15] to the equations for v_y. Since the y component is perpendicular to the shear plane,[16] it maintains a well-defined equilibrium distribution provided the shear rate is low:[17] $\dot\gamma\equiv 2U/h<1\tau^{-1}$, where h is the distance separating the walls. In our simulations, we used $\dot\gamma\le 0.16\tau^{-1}$ and verified that velocity profiles were essentially unchanged when the damping and Langevin terms were removed. The BC results were also independent of the values of U and h.

III. RESULTS

A. Layering normal to solid walls

Except as noted, our simulations were performed with systems containing $N_f=672$ fluid atoms and $N_w=192$ or 352 wall atoms. The latter correspond to $\rho_w/\rho=1$ and 2.52, respectively. An instantaneous atomic configuration, projected on to the xz plane, of a system under shear is shown in Fig. 1. The system measures $h=12.8\sigma$ between the walls, and 13.6σ by 5.1σ in the xy plane. The wall velocity and density, and the wall-fluid interaction are $U=1\sigma\tau^{-1}$, $\rho_w/\rho=2.52$, and $\varepsilon_{wf}/\varepsilon=1$, respectively.

Note the well-defined lattice structure of the solid walls. This induces both normal and parallel ordering in the adjacent fluid. Both types of ordering are independent of U for low shear rates.[7,17] We first consider normal ordering since it affects our study of the velocity fields, and previous work[7] had attempted to correlate it with flow BC's.

Normal ordering in LJ fluids is well understood.[18–20] Oscillations in the density are induced by structure in the fluid pair-correlation function $g(r)$, and the sharp cutoff in fluid density at the wall. Typical time-averaged density profiles observed in our systems are shown in Fig. 2. Near the wall there are well-defined fluid layers corresponding to density peaks. Beyond a distance of order 5σ the oscillations are negligible and one finds the unstructured density appropriate for a bulk liquid.

The magnitude of density oscillations is determined by

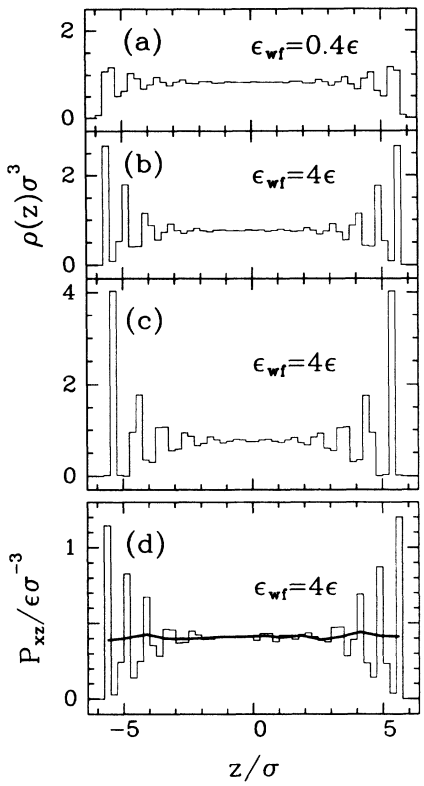

FIG. 2. Profiles normal to the wall of (a)–(c) density and (d) P_{xz} for $U=1\sigma\tau^{-1}$, $\langle \delta u^2 \rangle = 0$, and the indicated ϵ_{wf}. The wall density is $\rho_w=\rho$ except in (c) where $\rho_w=2.52\rho$. The heavy line in (d) represents P_{xz} averaged within fluid layers. The lighter line shows P_{xz} with a higher resolution.

two factors: the oscillations in $g(r)$, and the wall potential. Increasing the temperature reduces structure in $g(r)$ and thus in the density profile. Most of our simulations were done close to the melting temperature where the oscillations are largest. The wall potential determines how well-defined the first layer is, which in turn determines the size of successive oscillations. Note the sharp increase in normal ordering as ϵ_{wf} increases in Fig. 2. The larger the potential, the larger the energy cost of deviations from the favored position of the first layer.

Early analytical and numerical studies focused on systems with smooth continuum walls.[18,19] In these systems, the wall-fluid potential only depends on the distance z from the wall. Atomistic walls introduce corrugations in the potential felt by fluid atoms. This smears the first fluid layer, and thus reduces the density oscillations. Thermal roughness of the walls further decreases oscillations.

The structure normal to atomistic walls also depends on the competition between two length scales: The solid lattice constant and the molecular spacing of the fluid. This competition affects not only the amplitude of the oscillations but also the location of the layers. For example, as ϵ_{wf}/ϵ increases from 0.4 to 4 with $\rho_w/\rho=1$, the fluid layers become narrower and shift closer to the walls [Figs. 2(a) and 2(b)]. For larger wall densities, the fluid layers also sharpen as ϵ_{wf} increases, but their positions do not shift significantly towards the wall [Fig. 2(c)]. This density dependence can only be understood in the context of fluid structure parallel to the solid. A detailed analysis of the latter is presented in Sec. III C. Here we just note that increasing the wall density tends to decrease the effect of corrugations because fluid molecules are too big to fit in local minima of the wall potential. Thus the enhanced layering in Fig. 2(c) reflects both an increase in the effective wall-fluid interaction (more wall atoms) and a decrease in the effective in-plane corrugation.[21]

The density oscillations induce modulations normal to the solid walls in many other microscopic quantities, such as the velocity $V(\mathbf{r})=V_x(z)$ and the xz component of the microscopic pressure-stress tensor P_{xz}. The latter quantity is plotted in Fig. 2(d) for a simulation with $\epsilon_{wf}=4\epsilon$ and $\rho_w=\rho$. Note that peaks in P_{xz} coincide with peaks in the density [Fig. 2(b)]. The velocity gradient shows peaks *between* the layers.

Our goal is to determine boundary conditions for the equations of macroscopic hydrodynamics. For Couette flow, one expects on very general grounds that the normal stress transmitted through the fluid P_{xz} must be spatially constant. The Navier-Stokes equations (NSE's) further predict that $P_{xz}=\mu\partial V_x/\partial z=\text{const}$, where μ is the fluid viscosity. The oscillations on atomic scales in Fig. 2(d), and the apparent phase shift between oscillations in P_{xz} and the velocity gradient cannot be understood in terms of macroscopic fields and the NSE. However, this is not surprising since the equations of macroscopic hydrodynamics are derived assuming that quantities are averaged over scales larger than the mean free path.[22] In liquids this is of order the atomic separation σ. We find that averaging V and P_{xz} on this scale removes the oscillations [Fig. 2(d)]. Beyond the first or second layer, these smoothed quantities satisfy the Navier-Stokes equations with a constant viscosity. In some cases, the structure and the effective viscosity in the first fluid layers are modified as discussed below.

The velocities and other quantities presented in the following sections were averaged within bins corresponding to fluid layers. Averaging with Gaussian or other weighting functions produced similar results as long as the width was $\gtrsim\sigma$.

B. Velocity fields and slip length

Velocity profiles were computed for a wide range of parameters. A sample of our results is presented in Fig. 3 for three wall-fluid interactions and two wall densities. Squares indicate averages of V_x within layers, and solid lines are fifth-order polynomial fits through these values. The locations of the first layer of solid atoms on each side of the fluid correspond to the vertical borders of the plots. The dashed line in Fig. 3(b) represents the flow expected from hydrodynamic theory with a no-slip BC. Note that it is linear and reaches $\pm U$ at the walls.

Figure 3 clearly shows that flow near solid boundaries is strongly dependent on the strength of the wall-fluid interaction and on wall density. We first discuss the case of equal densities: $\rho_w/\rho=1$. For $\epsilon_{wf}/\epsilon=0.4$, the velocity

profile is linear with a no-slip BC [Fig. 3(a)]. As ε_{wf} increases, the magnitude of V_x in the layers nearest the wall increases and the profile becomes curved. At $\varepsilon_{wf}/\varepsilon=4$, $|V_x|/U=1.00\pm0.02$ in the first and second layers [Fig. 3(c)]. This implies that the first two fluid layers are locked to the solid wall. Similar locking has been observed in previous simulations.[4,5,9]

The flow boundary condition changes drastically for unequal wall and fluid densities. At weak wall-fluid interactions the velocity profile remains linear, but the magnitude at the wall is less than U. For example, at $\rho_w/\rho=2.52$ and $\varepsilon_{wf}/\varepsilon=0.4$ [Fig. 3(a)], the magnitude of the velocity at the wall is $0.64\pm0.03U$. This velocity difference between fluid and wall, or slip, decreases as the strength of the wall-fluid interaction increases. By $\varepsilon_{wf}/\varepsilon=1.8$ [Fig. 3(b)], the first fluid layer has partially locked to the solid wall, $|V_x|/U=0.95\pm0.01$. At sufficiently large interactions ($\varepsilon_{wf}/\varepsilon\gtrsim15$), up to two fluid layers lock to the solid, and the flow approaches that observed for equal wall and fluid densities. However, a regime was observed ($1.8\lesssim\varepsilon_{wf}/\varepsilon\lesssim6$) in which a large velocity gradient developed between the first and second fluid layers [Fig. 3(c)]—slip occurred between layers *within* the fluid. The origin of this behavior is described in Sec. III C.

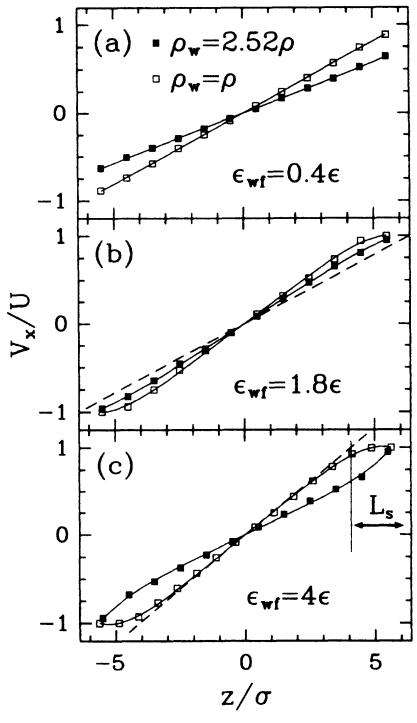

FIG. 3. Velocity profiles for $U=1\sigma\tau^{-1}$, $\langle\delta u^2\rangle=0$, and the indicated ε_{wf} and ρ_w. The locations of the first layers of solid atoms on each side of the fluid correspond to the vertical borders. Squares indicate averages of V_x within layers, and solid lines are fifth-order polynomial fits through these values. As shown in (c), the slopes of the fits at $z=0$ are used to define L_s. Note that L_s is negative for this case. The dashed line in (b) represents the flow expected from hydrodynamics with a no-slip BC ($L_s=0$).

The degree of slip associated with the velocity fields in Fig. 3 can be characterized by a length L_s. As shown in Fig. 3(c), we computed this quantity by extrapolating the flow field in the central region to U, and defining L_s as the distance from the solid wall to this point. A slip BC corresponds to $L_s>0$, while the usual no-slip BC corresponds to $L_s=0$. Negative values of L_s quantify the degree of locking between fluid and wall. The results of our analysis are presented in Fig. 4.

We first consider the effect of stiffness of the solid wall. Decreasing the stiffness increases thermal fluctuations in the wall, as well as its responsiveness to adjacent fluid atoms. As seen in Fig. 4, this increases L_s—the wall and fluid are more weakly coupled.

Figure 4 also shows that the wall and fluid are most strongly coupled (L_s is smallest) for $\rho_w/\rho=1$. This is not surprising since, as shown below, epitaxial locking is easiest at equal wall and fluid densities. One expects a perfect slip BC (i.e., $L_s\to\infty$) in the limit $\rho_w\to\infty$ since the wall is then effectively uncorrugated.

In general, L_s decreases with increasing ε_{wf} as expected. However, L_s becomes multivalued and may increase with ε_{wf} for $\rho_w/\rho=2.52$ and $1.8\lesssim\varepsilon_{wf}/\varepsilon\lesssim6$. As discussed above, the larger values of L_s in this range are not due to slip at the wall. Instead, slip occurs *between* fluid layers. For both $\rho_w/\rho=1$ and 2.52, L_s approaches $\sim2.3\sigma$ at large ε_{wf}.

These variations in L_s do not correlate well with the changes in fluid ordering *normal* to the solid walls. As ε_{wf} increases, the amplitude of the density oscillations increases and L_s decreases. One might thus conclude that greater order implies a stronger coupling and thus less slip. However, increasing ρ_w also enhances the fluid layering, but *increases* L_s. Indeed, continuum walls produce the largest degree of layering and complete slip. To understand this anticorrelation, the fluid structure *parallel* to the solid surface must be considered.

C. Fluid structure parallel to walls

We have carried out a detailed analysis of the structure within the fluid layers near the walls for different wall

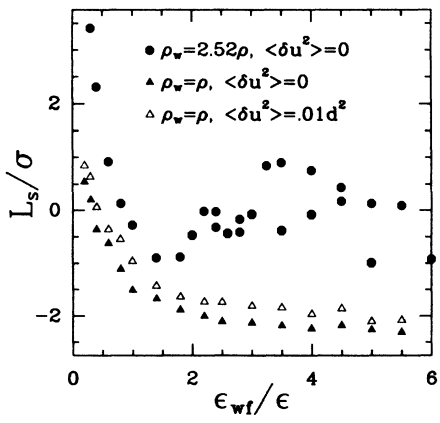

FIG. 4. L_s for various ε_{wf} at the indicated ρ_w and $\langle\delta u^2\rangle$.

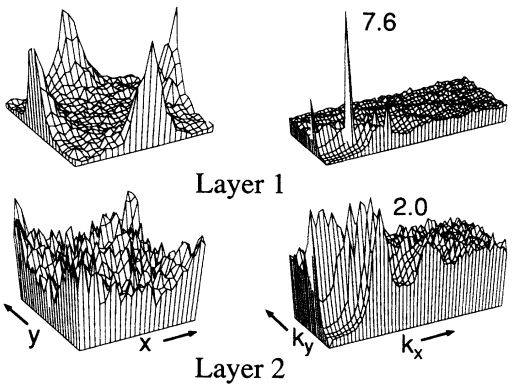

FIG. 5. $P(x,y)$ (left) and $S(k_x,k_y)$ (right) in the two fluid layers nearest the walls for $U=1\sigma\tau^{-1}$, $\varepsilon_{wf}=0.4\varepsilon$, $\rho_w=\rho$, and $\langle\delta u^2\rangle=0$. The scales vary and the heights of the largest peaks in $S(\mathbf{k})$ are indicated. Wall lattice sites lie at the center and corners of the unit cell for P.

properties and wall-fluid interactions. Two measures of the ordering were used. The first was the two-dimensional static structure factor $S(k_x,k_y)$ evaluated in the lth layer according to

$$S_l(\mathbf{k})=1/N_l\left|\sum_i e^{i\mathbf{k}\cdot\mathbf{r}_i}\right|^2, \tag{2}$$

where N_l was the number of fluid atoms within the layer. Note that the smallest possible resolution in k space is determined by the size of the system in the xy plane. We also calculated the spatial probability distribution $P_l(x,y)$ of fluid atoms in the lth layer relative to solid lattice sites. These lattice sites lie at the center and corners of the unit cell shown in Figs. 5–8. Both $S(\mathbf{k})$ and $P(\mathbf{r})$ were computed for the three fluid layers nearest the wall and averaged over 100τ.

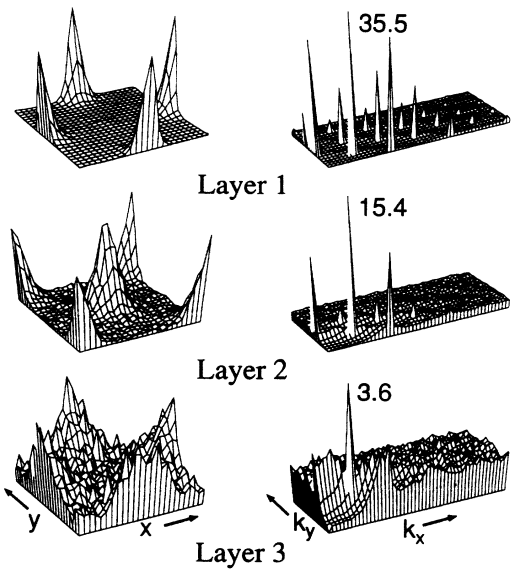

FIG. 6. $P(\mathbf{r})$ (left) and $S(\mathbf{k})$ (right) in the three fluid layers nearest the walls for the parameters of Fig. 5 except $\varepsilon_{wf}=1.8\varepsilon$.

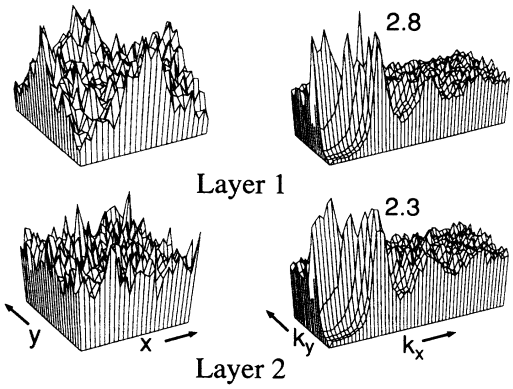

FIG. 7. $P(\mathbf{r})$ and $S(\mathbf{k})$ (right) in the two fluid layers nearest the walls for the parameters of Fig. 5 except $\rho_w=2.52\rho$.

Figure 5 shows $P(\mathbf{r})$ and $S(\mathbf{k})$ for $\varepsilon_{wf}/\varepsilon=0.4$, $\rho_w/\rho=1$, and $\langle\delta u^2\rangle=0$. This system satisfies the no-slip BC since $L_s\approx 0$. Self-diffusion in the xy plane within the first fluid layer is the same as in the bulk fluid. However, the solid induces modulations in $P(\mathbf{r})$. Peaks in P_1 are located at the centers of the sides of the unit cell, above gaps in the adjacent solid layer. Fluid atoms are 12 times more likely to sit over these gaps than directly over a wall atom. This induced ordering is also evident in $S_1(\mathbf{k})$, which shows several peaks. The main peak has magnitude 7.6. Note that increasing the thermal roughness of the solid or the temperature of the fluid reduces the degree of ordering. This is reflected in a broader spatial distribution, fewer harmonics in $S(\mathbf{k})$, and thus a larger L_s (Fig. 4).

Epitaxial locking of the first layer to the solid occurs at higher wall-fluid interactions. At $\varepsilon_{wf}=1.8\varepsilon$, the first layer has crystallized and is locked into the wall potential (Fig. 6). $P_1(\mathbf{r})$ shows that the fluid atoms in the first layer are well-localized about the centers of the sides of the unit cell. The mean-square displacement of a fluid atom from one of these sites, $\int r^2 P_1(\mathbf{r})d\mathbf{r}\sim 0.017d^2$, is below the Lindemann criterion for melting. $S_1(\mathbf{k})$ shows many

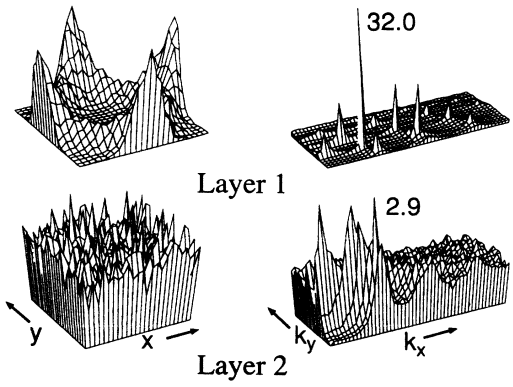

FIG. 8. $P(\mathbf{r})$ (left) and $S(\mathbf{k})$ (right) in the two fluid layers nearest the walls for the parameters of Fig. 6 except $\rho_w=2.52\rho$.

sharp Bragg peaks, including several higher-order harmonics. The magnitude of these peaks is consistent with the Debye-Waller factor[23] for the calculated mean-squared displacement. The peak heights scale with the number of particles per layer as expected for a solid. Final evidence for crystallization is the absence of measurable diffusion within the first layer.

The peaks in P and S become progressively smaller and broader in the second and third layers. Although the second fluid layer has not crystallized at $\varepsilon_{wf}/\varepsilon=1.8$, diffusion parallel to the wall is roughly half that in the bulk fluid. This layer crystallizes for $\varepsilon_{wf}/\varepsilon \gtrsim 3$. The third layer never crystallized in our simulations even for $\varepsilon_{wf}/\varepsilon=100$ and $r_c=3$. At this distance the ordering potential from the wall is dominated by that from the neighboring crystallized layers. Since this corresponds to the case $\varepsilon_{wf}=\varepsilon$, there is no epitaxy even when the second layer is completely crystallized. This explains the saturation of L_s in Fig. 4.

These crystallized layers correspond to a wetting phase between the solid wall and the liquid. As shown by Heinbuch and Fischer the number of solid layers decreases as T increases further above the melting temperature.[5] Solid wetting layers at solid-liquid interfaces are difficult to detect experimentally. However, solid wetting phases have been observed at many solid-gas interfaces.[24] As here, the phase typically extends over only a few atomic layers.

Very different structures within the fluid layers were observed in simulations with unequal wall and fluid densities. Figure 7 shows the results for $\varepsilon_{wf}/\varepsilon=0.4$, $\rho_w/\rho=2.52$, and $\langle \delta u^2 \rangle=0$. Note that the solid-induced modulations in $P_1(\mathbf{r})$ observed for $\rho_w/\rho=1$ are barely evident here. Consequently, it is not surprising that there is substantial slip: $L_s \approx 1.8$. Only for $\varepsilon_{wf} \gtrsim \varepsilon$ does the main peak in $S_1(\mathbf{k})$ exceed ~ 3 and L_s become negative.

In Fig. 8 we present results for $\varepsilon_{wf}/\varepsilon=1.8$. Note that the contact layer is only partially locked to the wall potential and there is no epitaxial ordering in the second layer. The ridge between peaks in $P_1(\mathbf{r})$ results from the incommensurability of fluid and solid layers. This mismatch makes it more difficult for the first fluid layer to move in towards the wall than in the case $\rho_w/\rho=1$ [Figs. 2(b) and 2(c)].

For $\varepsilon_{wf} \gtrsim 5$ the first layer forms one of a family of commensurate structures. An example is illustrated in Fig. 9, which is a time-averaged projection onto the xy plane, of all fluid atoms in the first layer for $\varepsilon_{wf}=5.5\varepsilon$, $\rho_w=2.52\rho$, and $\langle \delta u^2 \rangle=0$. The positions were averaged over 25τ at $U=0$. Note that the fluid has the same periodicity as the wall in the (11) direction, but a high-order (71/88) commensurate structure in the $(1\bar{1})$ direction. The dynamics of this structure are closely related to that of the well-studied Frenkel-Kontorova model.[25] It is only weakly pinned to the substrate potential along the high-order commensurate direction. In our sheared systems, the drag from adjacent fluid layers was sufficient to depin the structure leading to motion along the $(1\bar{1})$ direction. As ε_{wf} increased, the density of the first layer increased and it became more strongly pinned to the substrate. By

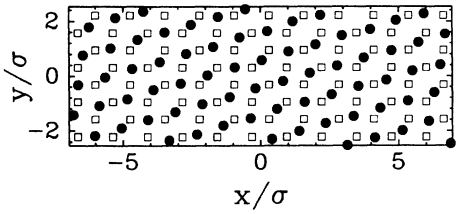

FIG. 9. Particle positions, projected on to the xy plane, of atoms in a wall layer (open squares) and adjacent fluid layer (closed circles) for $U=0$, $\varepsilon_{wf}=5.5\varepsilon$, $\rho_w=2.52\rho$, and $\langle \delta u^2 \rangle=0$. The positions were averaged over 25τ. Note that the fluid has the same periodicity as the wall in the (11) direction, but a high-order commensurate structure in the $(1\bar{1})$ direction.

$\varepsilon_{wf}/\varepsilon=15$ the densities of the wall and the first layer were equal and the first layer became completely locked: $|V_x|/U=1$.

There are two possible alignments of the high-order commensurate phases because of their broken symmetry. For $1.8 \lesssim \varepsilon_{wf}/\varepsilon \lesssim 5$ domains of each orientation coexisted. These domains were metastable and produced large fluctuations in the observed slip BC (Fig. 4). Presumably the fluctuations would average out in sufficiently large samples.

Thus far, we have shown that the qualitative features of fluid flow near solid boundaries can be understood in terms of structure induced in the fluid. We now extend this analysis by showing in a more quantitative fashion how L_s correlates with the in-plane structure. In Fig. 10, L_s is plotted against the main peak in the structure factor $S_1(\mathbf{G}_1)$, where $\mathbf{G}_1$ is the shortest reciprocal-lattice vector. Results are shown for $\rho_w/\rho=1$ and 2.52, $k_BT/\varepsilon=1.1$ and 1.4, $\langle \delta u^2 \rangle/d^2=0$ and 0.01, and $0.2 \leq \varepsilon_{wf}/\varepsilon \leq 25.0$. Note that for each density, values of L_s at different T and $\langle \delta u^2 \rangle$ collapse well onto a single curve. Moreover, for $L_s \gtrsim -1\sigma$ $[S_1(\mathbf{G}_1)/S_1(0)<0.3]$, the curves for different densities collapse. This is rather surprising since $\mathbf{G}_1$ is not the same in the two cases. The two densities only give different results at large $S_1(\mathbf{G}_1)$. In this limit the first layer is locked and the flow BC depends on the coupling between first and second fluid layers. This coupling is higher for $\rho_w=\rho$ because the two fluid layers have the same density. For $\rho_w/\rho=2.52$ and large ε_{wf}, the two densities are different and L_s is larger.

If we consider a locked first layer as part of the wall, $S_2(\mathbf{G}_1)$ should determine the slip boundary condition. To check this correlation, L_s was increased by 1 to reflect the locked first layer and plotted against $S_2(\mathbf{G}_1)$. The results for both wall densities fall near the other values in Fig. 10. Note that only systems with $S_1(\mathbf{G}_1)>0.5S(0)$ were considered. This includes all systems with $|V_x|/U=1$ in the first layer and a few systems with strongly pinned high-order commensurate structures.

The correlation between S and the flow boundary condition should not be surprising. The former reflects the

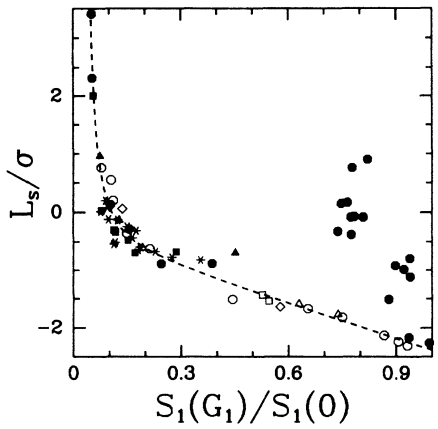

FIG. 10. Correlations between L_s and $S_1(\mathbf{G}_1)$ for systems with $k_BT/\varepsilon=1.1$ and $\langle\delta u^2\rangle/d^2=0$ (circles), and $\langle\delta u^2\rangle/d^2=0.01$ (diamonds); $k_BT/\varepsilon=1.4$ and $\langle\delta u^2\rangle/d^2=0$ (triangles), and $\langle\delta u^2\rangle/d^2=0.01$ (squares). The open and closed symbols indicate $\rho_w/\rho=1$ and 2.52, respectively. The starred points denote $S_2(\mathbf{G}_1)/S_2(0)$ and L_s+1 for those systems with $S_1(\mathbf{G}_1)>0.5S_1(0)$ and $L_s>-2\sigma$.

degree of positional correlation between atoms in the first truly fluid layer and those in the underlying solid. The latter reflects the effective viscous coupling between fluid and solid.

IV. SUMMARY AND CONCLUSIONS

In this paper, we have presented the first systematic study of the structure and flow of LJ fluids near solid boundaries. The effective BC for flow was quantified by a slip-length L_s. Both the structure and L_s varied widely with the wall geometry and the strength of the wall-fluid interaction.

The usual hydrodynamic no-slip BC ($L_s=0$) arose naturally for systems with equal wall and fluid densities. However, at large ε_{wf}, epitaxial ordering was induced in the first one or two fluid layers near the wall. These layers became locked to the wall and L_s was negative. Slip BC's ($L_s>0$) were only observed at very weak ε_{wf}.

Increasing the wall density decreased the effective corrugation of the wall, and reduced the amount of ordering within the fluid layers. This increased the amount of slip observed at small ε_{wf}. The system was only able to overcome the elastic cost of epitaxy at large wall-fluid interactions where commensurate structures formed in the first fluid layer. These structures were initially high-order commensurate in one direction. They were weakly pinned in this direction, and continued to slide relative to the solid. As ε_{wf} increased further, the density of the first layer increased to that of the solid and it became locked.

We showed that all of the changes in flow BC could be correlated to changes in the degree of order induced in the fluid. In particular, results for L_S for a variety of parameters were collapsed onto a single curve as a function of the magnitude of the largest peak in the in-plane structure factor S of the first nonlocked fluid layer.

The crystallized layers adjacent to the solid walls correspond to a wetting phase. In our simulation at most two layers of this phase formed. Experiments indicate that much thicker layers can form in some cases.[24] This would lead to large negative values of L_s.

Variations in fluid structure and flow near solid surfaces can have a large impact on single- and two-phase flow in confined geometries. For example, L_s determines the effective size of capillaries for single-phase flow and thus the permeability of porous media. Preliminary studies of moving contact lines,[26] intersections of fluid interfaces with solid surfaces, indicate that the amount of dissipation increases rapidly as L_s decreases. This may reflect the increase in the effective viscosity of the first few fluid layers. Sensitive dependence of dissipation at the contact line on fluid structure near the solid may explain the large differences in experimental results for homologous compounds.[27] Future work on single fluids should address how the shape as well as the size of fluid molecules affects flow BC's.

ACKNOWLEDGMENTS

We thank G. S. Grest, S. Hess, J. N. Israelachvili, and P. M. McGuiggan for useful discussions. Support from the National Science Foundation through Grant Nos. DMR 85-53271 and PHY 82-17853, and allocations at the National Center for Supercomputing Applications and Pittsburgh Supercomputing Center are gratefully acknowledged. M.O.R. also acknowledges support from the Sloan Foundation. P.A.T. acknowledges support from the Johns Hopkins University Applied Physics Laboratory.

[1]D. Y. C. Chan and R. G. Horn, J. Chem. Phys. **83**, 5311 (1985).
[2]E. Watts, J. Krim, and A. Widom, Phys. Rev. B **41**, 3466 (1990).
[3]J. N. Israelachvili, J. Colloid Interface Sci. **110**, 263 (1986).
[4]J. Koplik, J. Banavar, and J. Willemsen, Phys. Fluids A **1**, 781 (1989); Phys. Rev. Lett. **60**, 1282 (1988).
[5]U. Heinbuch and J. Fischer, Phys. Rev. A **40**, 1144 (1989).
[6]L. Hannon, G. C. Lie, and E. Clementi, Phys. Lett. A **119**, 174 (1986).
[7]I. Bitsanis, J. Magda, M. Tirrell, and H. Davis, J. Chem. Phys. **87**, 1733 (1987).
[8]C. Trozzi and G. Ciccotti, Phys. Rev. A **29**, 916 (1984).
[9]P. A. Thompson and M. O. Robbins, Phys. Rev. Lett. **63**, 766 (1989).
[10]See, for example, J. P. Hansen and I. R. McDonald, *Theory of Simple Liquids*, 2nd ed., (Academic, New York, 1986).
[11]M. Mareschal, M. Mansour, A. Puhl, and E. Kestement, Phys. Rev. Lett. **61**, 2550 (1988).
[12]See, for example, M. P. Allen and D. J. Tildesley, *Computer Simulation of Liquids* (Clarendon, New York, 1987).
[13]G. S. Grest, B. Dunweg, and K. Kremer (unpublished).
[14]D. J. Evans and G. P. Morriss, Phys. Rev. Lett. **56**, 2172

(1986).
[15]G. S. Grest and K. Kremer, Phys. Rev. A **33**, 3628 (1986).
[16]One exception to this occurred. For $\rho_w/\rho=2.52$ and intermediate wall-fluid interactions we observed $|v_y|\approx 0.05U$ near the wall. This finite velocity normal to the nominal shear plane stemmed from the formation of a high-order incommensurate structure adjacent to the wall (Sec. III C). We checked that our thermostat did not affect results in this case.
[17]W. Loose and S. Hess, Rheol. Acta. **28**, 91 (1989).
[18]S. Toxvaerd, J. Chem. Phys. **74**, 1998 (1981).
[19]J. Magda, M. Tirrell, and H. Davis, J. Chem. Phys. **83**, 1888 (1985).
[20]M. Schoen, J. Cushman, D. Diestler, and C. Rhykerd, Jr., J. Chem. Phys. **88**, 1394 (1988).
[21]In addition to enhanced layering, the fluid gets drawn in towards the wall as the ε_{wf} and ρ_w increase. Due to the finite size of our simulation cell, this caused nearly a 10% decrease in density and 25% decrease in viscosity of the bulk fluid as $\varepsilon_{wf}/\varepsilon$ varied from 0.4 to 5.0. However, simulations with systems twice as large between the walls revealed no substantial changes in the flow fields and in the fluid structure near the wall.
[22]Indeed thermodynamic fields such as P_{xz} can only be defined on these scales.
[23]See, for example, C. Kittel, *Quantum Theory of Solids* (Wiley, New York, 1963).
[24]J. Krim, J. G. Dash, and J. Suzanne, Phys. Rev. Lett. **52**, 640 (1984); S. K. Satija, M. Sutton, R. J. Birgeneau, H. Hong, L. Passell, and J. P. Wicksted, Phys. Rev. B **35**, 2064 (1987), and references therein.
[25]P. Bak, Rep. Prog. Phys. **45**, 587 (1982); S. N. Coppersmith, Phys. Rev. A **36**, 3375 (1987).
[26]M. O. Robbins and P. A. Thompson, *Macromolecular Liquids*, edited by C. R. Safinya, S. A. Safran, and P. A. Pincus (Materials Research Society, Pittsburgh, 1990), p. 411.
[27]M. Fermigier and P. Jenffer (unpublished).